Hydrothermal synthesis of magnetite: investigation of influence of aging time and mechanism

Xiaoning Sun[1,2], *Kangning Sun*[1,2], *Yanjie Liang*[1,2]

[1]*Key Laboratory for Liquid-Solid Structural Evolution and Processing of Materials (Ministry of Education), Shandong University, Jinan 250061, People's Republic of China*
[2]*Key Laboratory of Engineering Ceramics, Shandong University, Jinan 250061, People's Republic of China*
E-mail: sunkangning@sdu.edu.cn

Published in Micro & Nano Letters; Received on 16th June 2014; Revised on 21st September 2014; Accepted on 9th December 2014

Magnetite (Fe_3O_4) particles are prepared by a hydrothermal method using ethylene glycol as the solvent. Aging time is a very important factor in the reaction process. The properties and morphology of the products with different aging times are investigated. In the initial stage of the reaction (1 and 2 h), the main powders were iron hydroxides. Fe_3O_4 particles generated (3 h) and grew into spherical shapes (4–10 h) with the extended aging time. The particle size and the specific saturation magnetisation also varied with aging time. By analysing the powders and the liquids during the reaction, a probable mechanism is studied.

1. Introduction: Magnetic materials have aroused considerable attention in the past decades because of their potential applications in the communication, storage, mechanics and biomedical fields [1–4]. Magnetite (Fe_3O_4) has attracted the most attention because of its excellent magnetic properties, good biocompatibility and low toxicity [5–7].

There are plenty of methods to synthesise Fe_3O_4, such as the microemulsion method [8, 9], coprecipitation method [10], gel–sol method [11], high-temperature decomposition method [12], hydrothermal method [13] and so on. The hydrothermal process has been proven to be an effective and convenient method to prepare many kinds of single crystals with different morphologies and functions. The high temperature and high pressure in the autoclave result in rapid nucleation and faster growth of the newly formed particles, leading to the formation of small-sized particles [14–16].

Deng *et al.* [17] prepared single-crystal ferrite microspheres by a hydrothermal method using ethylene glycol as the solvent and reducing agent, this synthetic method is easy to operate with no requirement of protective gas to avoid the oxidation of Fe^{2+}; therefore, it is widely used now. The physical and chemical properties of the products are greatly affected by the synthesis parameters in this process. Jean *et al.* [18] found that the size and morphology of the Fe_3O_4 powders were influenced by the Fe^{3+} concentration. The amount of sodium acetate also affected the size and the morphology of the final products, which were investigated by Zhang *et al.* [19].

The effect of aging time on powder synthesis is studied in some papers [20, 21]. However, there are few researches on the aging time in the process of hydrothermal synthesis. In this context, we focus on the role of aging time in the hydrothermal process of preparing magnetic particles. The influence of aging time on the morphology and magnetic properties is presented. Furthermore, we discuss a possible formation process of Fe_3O_4.

2. Experimental

2.1. Synthesis: A measure of 5 mmol of ferric chloride ($FeCl_3{\cdot}6H_2O$) was dissolved in 20 ml of ethylene glycol ($C_2H_6O_2$) to form a clear solution. Then 3.6 g of sodium acetate (CH_3COONa) and 4 ml of polyethylene glycol-200 were added into the above solution. After the mixture was stirred vigorously for 30 min, the solution was transferred into a Teflon-lined stainless-steel autoclave (50 ml capacity), and heated at 200°C for different times. The detailed preparation conditions are listed in Table 1. As the autoclave was cooled in air to room temperature, the obtained products were centrifuged and washed with deionised water and ethanol three times. Then the samples were dried at 60°C and finally ground to powders.

2.2. Characterisation: X-ray diffraction (XRD) patterns were characterised on a Rigaku Dmax-rc diffractometer with Ni-filtered Cu Kα radiation ($V = 50$ kV, $I = 80$ mA). Fourier transform infrared spectroscopy (FTIR) was conducted on a Bruker Vertex 70 spectrometer over a range of 400–4000 cm^{-1} at a resolution of 4 cm^{-1}. The size and morphologies of the powders were analysed using a Hitachi SU-70 scanning electron microscope (Hitachi company, Japan), which was operated at 5–20 kV. An energy-dispersive spectrometer unit attached to the Hitachi SU-70 scanning electron microscope was used to verify the elements of the powders. Magnetic properties were studied using a JDM-13E vibrating sample magnetometer with a maximum magnetic field of 15 kOe at 298 K.

3. Results and discussion: The XRD patterns of samples S1–S10 are shown in Fig. 1. The diffraction peaks of S1 and S2 are excessive, broad and difficult to be distinguished, indicating the crystallinity of powders are poor (Fig. 1*a*). As shown in the energy-dispersive spectrometer (EDS) graph, the main elements are Fe and O (Fig. 2, H cannot be detected by EDS). We consider the diffraction peaks at about 24°, 36° and 48° represent $Fe(OH)_3$ (JCPDS File No. 46-1436), FeOOH (lepidocrocite, JCPDS File No. 44-1415) and FeO(OH) (ferrihydrite, JCPDS File No. 46-1315), respectively. This indicates the initial products of the reaction were ferric hydroxides. Characteristic diffraction peaks of Fe_3O_4 appear in S3, which means the formation of Fe_3O_4 (Fig. 1*a*). The diffraction intensities of Fe_3O_4 are enhanced in S4–S10. Meanwhile, the characteristic peaks of ferric hydroxides disappear, all peaks match well with the structure of Fe_3O_4 (JCPDS File No. 75-1609). These results show that ferric hydroxides are completely transformed into well-crystallised Fe_3O_4 (Figs. 1*b* and *c*).

The morphological changes of the samples were observed by scanning electron microscope (SEM) to compare the structural results obtained by XRD. Fig. 3 demonstrates that the aging time has a significant effect on the morphology and size of the products. The granules of S1 exhibit large size and irregular polygon shapes (Fig. 3*a*), while they obtain smaller size and smoother shapes in S2 (Fig. 3*b*). A remarkable difference is found in Fig. 3*c* (S3), spheres

Table 1 Aging time of samples

Samples	S0	S1	S2	S3	S4	S5	S6	S7	S8	S9	S10
aging time, h	0	1	2	3	4	5	6	7	8	9	10

with diameters of about 200 nm are formed on the surface. In addition, the SEM micrographs of S4–S10 contain Fe_3O_4 spheres only (Figs. 3*d–j*). These are in accordance with the XRD profiles.

Fig. 4 is the FTIR spectra of the mix solution of S0 and the upper liquid of S6. Most of the functional groups represented by the peaks are indicated in the Figure. Comparing the two curves, the peak at 1713 cm^{-1} in S0 moved to 1726 cm^{-1} in S6, which is attributed to the transform of a carboxy group to an aldehyde group. Moreover, there are two new peaks at 2119 and 1943 cm^{-1} in S6, they are assigned to the vibration of C°C triple bond and C=C=C double bond.

$FeCl_3{\cdot}6H_2O$ that dissolves in $C_2H_6O_2$ will form a weak yellow transparent solution. When CH_3COONa was added into the above solution, we observed a reddish-brown precipitate, which testified that a new product was formed. If there was no CH_3COONa, there would no particles generated in the end. Meanwhile, the ratio of $FeCl_3$ to CH_3COONa must be lower than 1:3; otherwise reddish-brown products would appear, which is regarded as

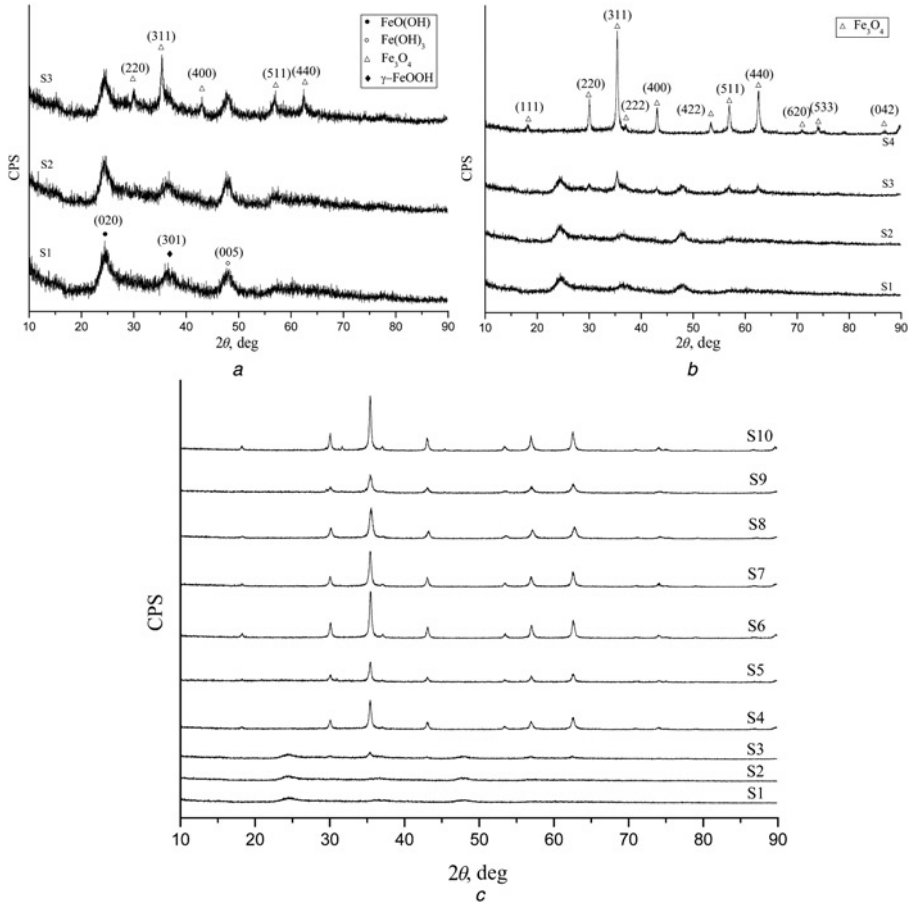

Figure 1 *XRD patterns of samples*
a S1–S3
b S1–S4
c S1–S10

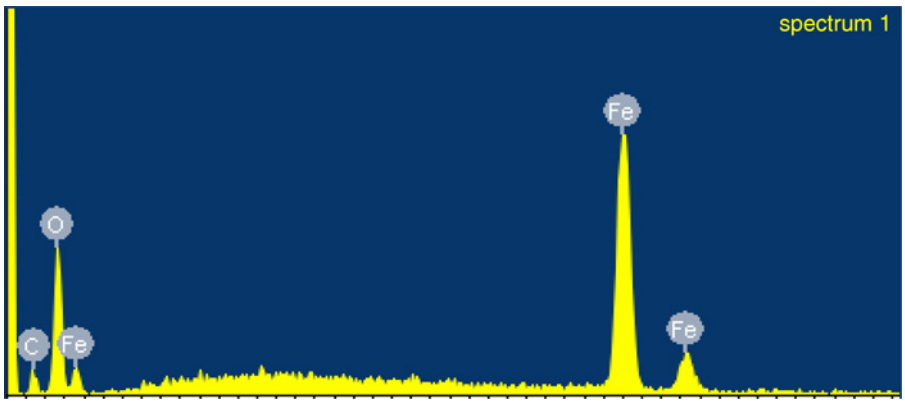

Figure 2 *EDS spectra of S1*

doi: 10.1049/mnl.2014.0344

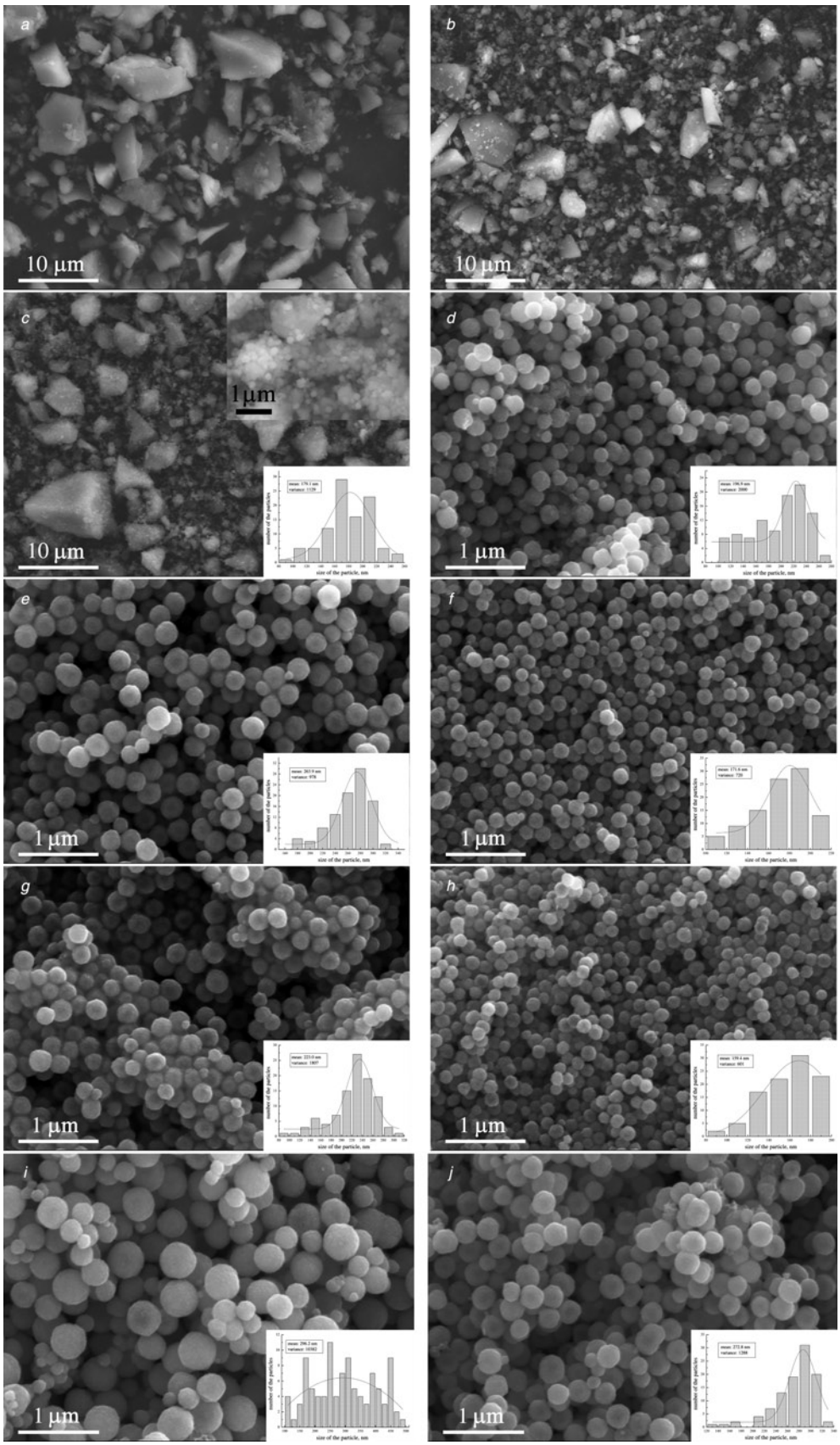

Figure 3 *SEM images and size distribution of samples a–j* S1–S10

Fe_2O_3. These show that CH_3COONa plays an important role in the Fe_3O_4 formation process; it would react with $FeCl_3$ to form an intermediate. The vibrations of C≡C and C=C=C indicate that there may be an elimination reaction of $C_2H_6O_2$ in the reaction. On account of this, there is occurrence of an aldehyde group in the spectra; we suppose that the new product in the upper liquid is

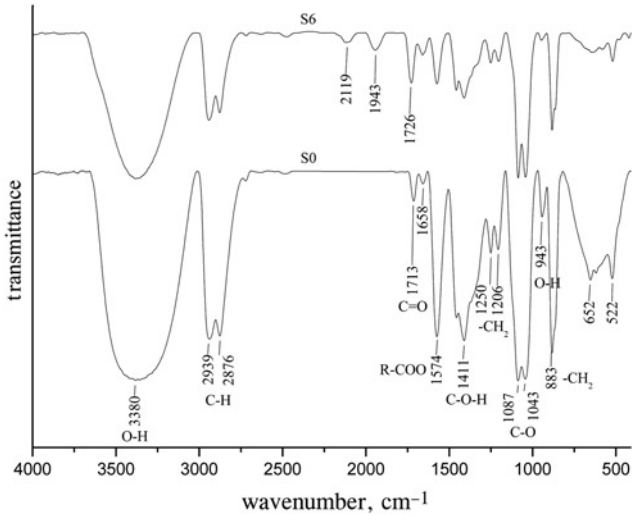

Figure 4 *FTIR spectra of solutions of S0 and S6*

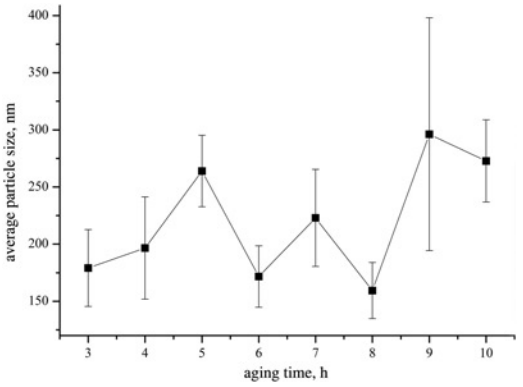

Figure 5 *Dependence of average particle size and standard deviation on the aging time of samples S3–S10*

$HOCH_2CHO$. XRD analysis showed that the prime powders are ferric hydroxide, and then turn into Fe_3O_4. To generate Fe_3O_4, ferrous and ferric irons are required. However, there is no characteristic diffraction peaks of ferrous hydroxide in Fig. 1; this is probably because of the oxidation of ferrous hydroxide into ferric hydroxide. On the basis of the above-mentioned analysis results, the possible reaction process is

$$FeCl_3 + 3CH_3COONa \rightarrow Fe(CH_3COO)_3 + 3NaCl \quad (1)$$

$$Fe(CH_3COO)_3 + 3H_2O \rightarrow 3CH_3COOH + Fe(OH)_3 \quad (2)$$

$$2HOCH_2CH_2OH \rightarrow HOCH_2 - CH{=}C{=}CH_2 + 3H_2O \quad (3)$$

$$HOCH_2CH_2OH \rightarrow CH{\equiv}CH + 2H_2O \quad (4)$$

$$Fe(OH)_3 + HOCH_2CH_2OH \rightarrow Fe(OH)_2 + CH_2CHO + 2H_2O \quad (5)$$

$$2Fe(OH)_3 + Fe(OH)_2 \rightarrow Fe_3O_4 + 4H_2O \quad (6)$$

In our research, within the aging time limit of 4–10 h, the change of

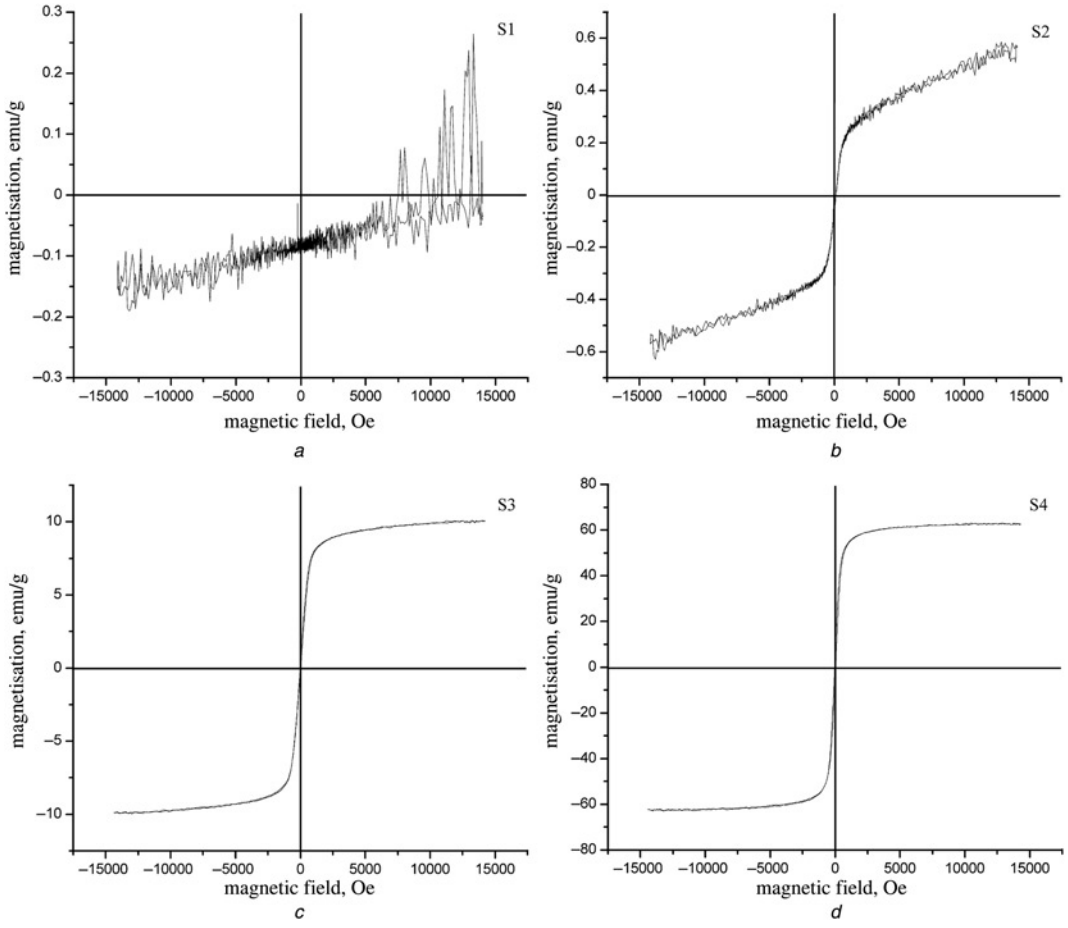

Figure 6 *Specific saturation magnetisations of samples S1–S4 (Figs. 6a to d, respectively)*

doi: 10.1049/mnl.2014.0344

particle size was complicated (Figs. 3*d–j*). The size first increases, then decreases and increases finally, which presents a regular cycle of change with aging time, shown in Fig. 5. Therefore, we conclude the growth mechanism of Fe_3O_4 particles as follows.

The high temperature and pressure environment will spur the thermal motion of molecules. When the concentration of the solute in the solution is higher than that of the grain nucleation needed, it begins to nucleate and growth occurs. The increase in particle size was because of the chemical reaction in the system at this moment. In this Letter, Fe_3O_4 began to nucleate when the aging time was 3 h (Fig. 3*c*). Then the products completely transformed into Fe_3O_4 when the aging time was 4 h. Random aggregation of the resultant crystallites minimised the total interfacial energy, leading to a spherical structure (Fig. 3*d*). As there were no other products except Fe_3O_4, we consider the system was in equilibrium when the aging time goes to 5 h. According to Ostwald ripening, as smaller particles hold higher interfacial energy than bigger particles, there is a tendency for smaller particles to dissolve into the surrounding medium and precipitate on the surface of larger particles and larger ones to grow, by the transfer of the solute through the solvent from particle to particle [22]. Therefore, the particle size grew bigger in S5, S7 and S9. The sealed autoclave can be considered as a closed system. The water generated in the reaction will be gasified at 200°C, which could alter the gas pressure of the system and break the balance of dissolution and precipitation in the Fe_3O_4 formation process. These changes make the reactions proceed in the opposite direction; the grown particles dissolve again and become small, as seen in S6, S8 and S10. As the steady temperature of the system offers energy for continuous crystal growth, the crystallite size and the particle size will increase when aging for a long time [17].

The specific saturation magnetisations (σ_s) of S1–S4 are shown in Fig. 6; the results agree with the results of XRD and SEM. The curve is disorderly and unsystematic at first because the main products are iron hydroxide. When a tiny amount of Fe_3O_4 emerged in the products, the curve became symmetrical. Distinct Fe_3O_4 particles are observed in S3; therefore, the curve turns into a typical magnetic hysteresis loop with low σ_s. Prolonging the aging time to 4 h or more, σ_s increases rapidly because of the good crystallisation of Fe_3O_4. The σ_s can reach up to 71.42 emu/g. The average crystallite sizes that are calculated based on the XRD patterns and the specific saturation magnetisations of S4–S10 are shown in Fig. 7. It is clearly seen that σ_s has almost the same changing trend with the dimensional variation of crystallite, which can be explained by the research that the magnetic properties of magnetite particles strongly depend on their crystallite size and the structure [23–25].

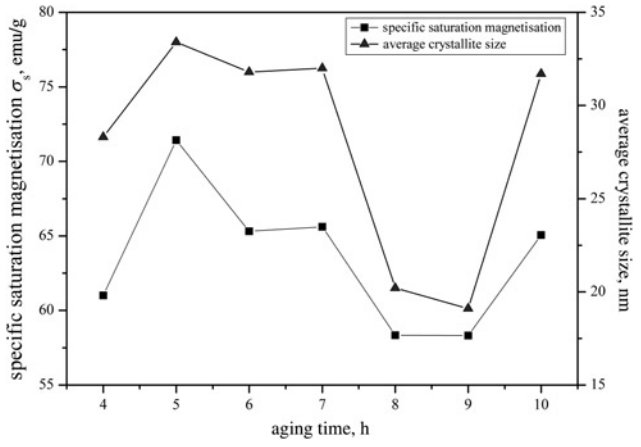

Figure 7 *Average crystallite size and specific saturation magnetisation of samples with different aging times: S4–S10*

4. Conclusion: Aging time plays an important role in the formation of Fe_3O_4 and grain growth. The products change from iron hydroxide to Fe_3O_4 with the extension of aging time. The sizes of Fe_3O_4 spheres also vary with aging time, which can be illustrated by the Ostwald ripening and chemical equilibrium. The specific saturation magnetisations of the particles are greatly affected by the products and the crystallite size. Therefore, to obtain Fe_3O_4 with proper size and σ_s, aging time should be controlled carefully. A possible reaction process is given according to the test results.

5. Acknowledgments: The authors acknowledge the support of the Natural Science Foundation of China (grant nos. 81171463 and 30870610) and the School of Material Science and Engineering, Shandong University.

6 References

[1] Wang S., Sun N., Yamaguchi M., Yabukami S.: 'Sandwich films: properties of a new soft magnetic material', *Nature*, 2000, **407**, (6801), pp. 150–151

[2] Kim D.-Y., Bae H.-S., Park M.-K., *ET AL.*: 'A study of magnetic fluid seals for underwater robotic vehicles', *Int. J. Appl. Electromagn. Mech.*, 2010, **33**, (1), pp. 857–863

[3] Frey N.A., Peng S., Cheng K., Sun S.: 'Magnetic nanoparticles: synthesis, functionalization, and applications in bioimaging and magnetic energy storage', *Chem. Soc. Rev.*, 2009, **38**, (9), pp. 2532–2542

[4] Kumar C.S., Mohammad F.: 'Magnetic nanomaterials for hyperthermia-based therapy and controlled drug delivery', *Adv. Drug Delivery Rev.*, 2011, **63**, (9), pp. 789–808

[5] Huang H.-C., Barua S., Sharma G., Dey S.K., Rege K.: 'Inorganic nanoparticles for cancer imaging and therapy', *J. Controlled Release*, 2011, **155**, (3), pp. 344–357

[6] Ankamwar B., Lai T., Huang J., *ET AL.*: 'Biocompatibility of Fe_3O_4 nanoparticles evaluated by in vitro cytotoxicity assays using normal, glia and breast cancer cells', *Nanotechnology*, 2010, **21**, (7), p. 075102

[7] Samanta B., Yan H., Fischer N.O., Shi J., Jerry D.J., Rotello V.M.: 'Protein-passivated Fe_3O_4 nanoparticles: low toxicity and rapid heating for thermal therapy', *J. Mater. Chem.*, 2008, **18**, (11), pp. 1204–1208

[8] Liu Z., Wang X., Yao K., *ET AL.*: 'Synthesis of magnetite nanoparticles in W/O microemulsion', *J. Mater. Sci.*, 2004, **39**, (7), pp. 2633–2636

[9] Liz L., Quintela M.L., Mira J., Rivas J.: 'Preparation of colloidal Fe_3O_4 ultrafine particles in microemulsions', *J. Mater. Sci.*, 1994, **29**, (14), pp. 3797–3801

[10] Sun J., Zhou S., Hou P., *ET AL.*: 'Synthesis and characterization of biocompatible Fe_3O_4 nanoparticles', *J. Biomed. Mater. Res. A*, 2007, **80**, (2), pp. 333–341

[11] Itoh H., Sugimoto T.: 'Systematic control of size, shape, structure, and magnetic properties of uniform magnetite and maghemite particles', *J. Colloid Interface Sci.*, 2003, **265**, (2), pp. 283–295

[12] Roca A., Morales M., O'Grady K., Serna C.: 'Structural and magnetic properties of uniform magnetite nanoparticles prepared by high temperature decomposition of organic precursors', *Nanotechnology*, 2006, **17**, (11), p. 2783

[13] Ni S., Lin S., Pan Q., Yang F., Huang K., He D.: 'Hydrothermal synthesis and microwave absorption properties of Fe_3O_4 nanocrystals', *J. Phys. D, Appl. Phys.*, 2009, **42**, (5), p. 055004

[14] Chen F., Gao Q., Hong G., Ni J.: 'Synthesis and characterization of magnetite dodecahedron nanostructure by hydrothermal method', *J. Magn. Magn. Mater.*, 2008, **320**, (11), pp. 1775–1780

[15] Ge S., Shi X., Sun K., *ET AL.*: 'Facile hydrothermal synthesis of iron oxide nanoparticles with tunable magnetic properties', *J. Phys. Chem. C*, 2009, **113**, (31), pp. 13593–13599

[16] Yu S., Wan J., Yu X., Chen K.: 'Preparation and characterization of hydrophobic magnetite microspheres by a simple solvothermal method', *J. Phys. Chem. Solids*, 2010, **71**, (3), pp. 412–415

[17] Deng H., Li X., Peng Q., Wang X., Chen J., Li Y.: 'Monodisperse magnetic single–crystal ferrite microspheres', *Angewandte Chem.*, 2005, **117**, (18), pp. 2842–2845

[18] Jean M., Nachbaur V., Le Breton J.-M.: 'Synthesis and characterization of magnetite powders obtained by the solvothermal method: influence of the Fe^{3+} concentration', *J. Alloys Compnd.*, 2012, **513**, pp. 425–429

[19] Zhang W., Shen F., Hong R.: 'Solvothermal synthesis of magnetic Fe_3O_4 microparticles via self-assembly of Fe_3O_4 nanoparticles', *Particuology*, 2011, **9**, (2), pp. 179–186

[20] Alfaro S., Rodriguez C., Valenzuela M., Bosch P.: 'Aging time effect on the synthesis of small crystal Lta zeolites in the absence of organic template', *Mater. Lett.*, 2007, **61**, (23), pp. 4655–4658
[21] Gubicza J., Lábár J.L., Quynh L.M., Nam N.H., Luong N.H.: 'Evolution of size and shape of gold nanoparticles during long-time aging', *Mater. Chem. Phys.*, 2013
[22] Ostwald W.: 'Studies on formation and transformation of solid materials', *Z. Phys. Chem.*, 1897, **22**, pp. 289–330
[23] Han D., Wang J., Luo H.: 'Crystallite size effect on saturation magnetization of fine ferrimagnetic particles', *J. Magn. Magn. Mater.*, 1994, **136**, (1), pp. 176–182
[24] Dyakonov V., Ślawska-Waniewska A., Kazmierczak J., *ET AL.*: 'Nanoparticle size effect on the magnetic and transport properties of (Lasr) Mno manganites', *Low Temperature Phys.* 2009, **35**, p. 568
[25] Xuan S., Wang Y.-X.J., Yu J.C., Cham-Fai Leung K.: 'Tuning the grain size and particle size of superparamagnetic Fe_3O_4 microparticles', *Chem. Mater.*, 2009, **21**, (21), pp. 5079–5087

doi: 10.1049/mnl.2014.0344